Journal of Alloys and Compounds 826 (2020) 154075

Contents lists available at ScienceDirect

Journal of Alloys and Compounds

journal homepage: http://www.elsevier.com/locate/jalcom

Mechanical properties and strain hardening behavior of aluminum matrix composites reinforced with few-walled carbon nanotubes

B. Chen [a, *], Z. Li [a], J. Shen [b, c], S. Li [d], L. Jia [d], J. Umeda [b], K. Kondoh [b], J.S. Li [a]

[a] State Key Laboratory of Solidification Processing, Northwestern Polytechnical University, Xi'an, 710072, Shaanxi, China
[b] Joining and Welding Research Institution, Osaka University, 11-1 Mihogaoka, Ibaraki, Osaka, 567-0047, Japan
[c] School of Aeronautics, Northwestern Polytechnical University, Xi'an, 710072, Shaanxi, China
[d] School of Materials Science and Engineering, Xi'an University of Technology, Xi'an, 710048, China

ARTICLE INFO

Article history:
Received 17 October 2019
Received in revised form
17 January 2020
Accepted 26 January 2020
Available online 30 January 2020

Keywords:
Metal matrix composites (MMCs)
Carbon nanotubes (CNTs)
Strength
Ductility
Strain hardening

ABSTRACT

In this study, for the first time few-walled carbon nanotubes (FWCNTs) with ~3 walls were used as reinforcements in fabricating high performance aluminum matrix composites (AMCs). FWCNTs/Al composites and referential Al materials were prepared by a powder metallurgy route consisting of high energy ball milling, spark plasma sintering (SPS) and subsequent hot extrusion. It is found that, by decreasing SPS temperature and time, FWCNTs/Al composites showed reduced grains with an increased dislocation density and improved structural integrity of FWCNTs, leading to an increased tensile strength. Meanwhile, comparatively high strain hardening rates and long strain softening behavior were observed after necking in the sample sintered at 500 °C, which resulted in a tensile elongation of 11.7% with a high yield strength of 382 MPa. The experimental results suggested that, compared with traditional multi-walled carbon nano-tubes (MWCNTs), FWCNTs showed a noticeably enhanced strengthening effect and provided a good balance of strength and ductility in Al composites. It may make FWCNTs a good reinforcement candidate for metal matrix composites to achieve improved mechanical properties.

1. Introduction

Aluminum (Al) and its alloys are key materials in aerospace and other transportation fields due to their excellent properties such as high specific strength, high thermal conductivity and excellent corrosion resistance. With the increasing properties required by modern aircrafts and cars, traditional Al alloys gradually fail to satisfy the demand of high performances. The Al alloys-based composites not only inherit the excellent properties of Al alloys, but also can have high specific modulus, good high-temperature performances, low thermal expansion coefficient, good fatigue resistance and wear resistance that contributed by reinforcements [1]. Thus, Al matrix composites (AMCs) progressively become an important class of materials in aerospace and automobile areas [2]. A simple and easy path to improve the properties of AMCs is to wisely select the reinforcing phase. Carbon nanotubes (CNTs) are known for their low density, large aspect ratio, high specific surface area, ultra-high strength (up to ~100 GPa), ultra-high modulus (~1 TPa) and excellent thermal/electrical properties [3], which then are popularly used and studied in Al composites [4,5]. The ever-obtained results have implied that the CNT-reinforced AMCs are expected to become the next generation of lightweight and high-strength structural materials.

According to the shear-lag theory [6,7], to achieve a high strength of AMCs, CNTs with high strength and large aspect ratios are desired. As revealed in previous studies [8,9], the strength and aspect ratio of CNTs can be simultaneously increased by reducing the number of walls. Therefore, from the viewpoint of theoretical prediction, the most promising CNTs to show strengthening effect most efficiently shall be single-walled CNTs (SWCNTs). Yet, in reality it is rather difficult to produce SWCNTs with high aspect ratios in massive production. Moreover, SWCNTs are quite difficult to disperse uniformly that may cause agglomeration and reduce their strengthening efficiency. A previous study reported that the strengthening effect of SWCNTs in the 5083 Al alloy matrix was even inferior to multi-walled CNTs (MWCNTs) [10]. As a result, MWCNTs with much larger diameters (several tens of nanometers) were used as reinforcements in most of studies on CNTs/Al composites [11–14], mainly owing to their cost-efficient production and easy dispersion. To demonstrate the effect of CNT diameters, Esawi

* Corresponding author.
E-mail addresses: chen@nwpu.edu.cn, biao.chen521@gmail.com (B. Chen).

https://doi.org/10.1016/j.jallcom.2020.154075
0925-8388/

et al. [15] compared the strengthening effect of two multi-walled CNTs with different diameters of 40 nm and 140 nm. The results showed that the CNT diameter has a great effect on dispersion quality and consequent strength of composites. Therefore, an improved strengthening effect shall be achieved by a careful selection of CNT types with optimized balance of CNT diameter and strength.

As a compromise, few-walled CNTs (FWCNTs, with a wall number of <10) is a wise choice since they have a strength comparable to that of SWCNTs [16] while having an aspect ratio for easy dispersion. Yet, the strengthening efficiency of FWCNTs has been hardly studied yet, not to speak of the optimized processing route for FWCNTs/Al composites. In this study, an attempt was made to investigate the strengthening effect of FWCNTs in AMCs, as well as the appropriate parameters for materials production. FWCNTs of ~3 walls (~5 nm in diameter) were uniformly dispersed into Al powders by high energy ball milling, and then the powder mixture was consolidated by spark plasma sintering (SPS) under different conditions followed by hot extrusion. The results showed that FWCNTs/Al composites had an enhanced balance of strength and ductility. It is also found that the CNT type and SPS condition both have a great effect on the strengthening and strain hardening behavior of CNTs/Al composites. The underlying mechanism was discussed in relating to their microstructures with an assistance of proper strengthening and strain hardening models.

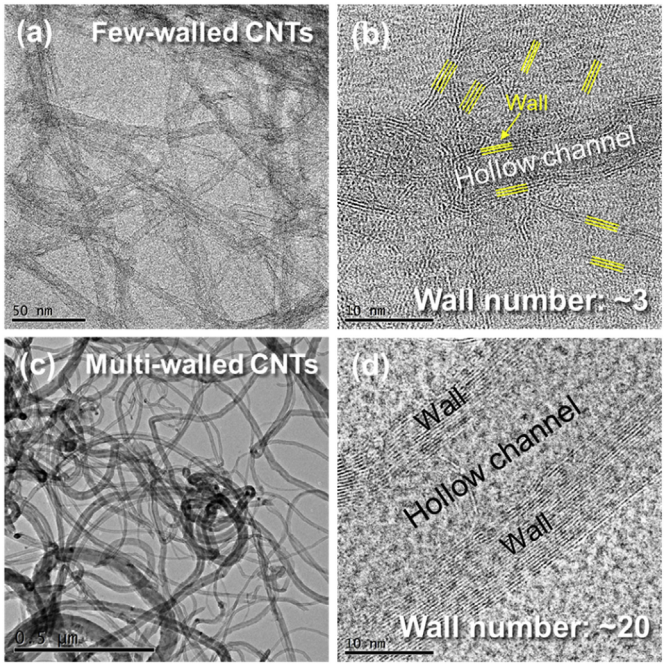

Fig. 1. High-resolution TEM images of raw FWCNTs (a, b) and MWCNTs (c, d) at different magnifications. Marked parallel lines in (b) suggest CNT walls.

2. Experimental methods

2.1. Powder processing

In this study, FWCNTs (~3 walls, ~5 nm in diameter and ~1 μm in length) powders and pure Al powders (120 g, ~20 μm in diameter, 99.9% in purity) were mixed by high energy ball milling (HEBM) using a planetary ball milling machine (PULVERISETTE 5, Fritsch, Germany). The FWCNTs (1 wt%) powders and process control agent (stearic acid, 1 wt%) were sealed with Al powders in a ZrO_2 jar (500 mL in volume), where ZrO_2 milling balls of 10 mm in diameter with a ball to powder ratio of 5:1 were used. The revolution speed was 200 rpm and the milling time was 24 h. To suppress extensive oxidation of powders, the milling jar was aerated with a flow of argon gas and a cooling-down break of 5 min in every 15 min to avoid overheating. One sample doped with commonly used MWCNTs (~20 walls, ~15 nm in diameter and ~1 μm in length) was used as reference. The morphologies of FWCNTs powders and MWCNTs powders are shown in Fig. 1. The structure of walls and hollow channels of FWCNTs and MWCNTs can be clearly observed in the high-resolution TEM view (Fig. 1b, d). There is an obvious difference in the wall number and outer-diameter between the two types of CNTs.

2.2. Composite fabrication

The as-received FWCNTs/Al powder mixture (60 g) was consolidated by spark plasma sintering (SPS) in vacuum (<5 Pa) at two conditions, 600 °C for 60 min and 500 °C for 30 min, for which the corresponding samples are named as SPS600C and SPS500C for simplicity hereafter. To further improve the composite density, a hot-extrusion process was applied to the sintered billet. Referential materials made of raw pure Al powders, milled Al powders and MWCNT-Al powders were also consolidated under the same conditions, hereafter named as pure Al, milled Al and MWCNT/Al composite, respectively. More details of the HEBM process can be found elsewhere [17,18].

2.3. Microstructure characterization

A field emission scanning electron microscopy (FE-SEM, JEM-6500F, JEOL, Japan) was used to characterize the morphology of Al-FWCNT powders and composites. In addition, a high-resolution transmission electron microscope (HRTEM, JEM-2010, JEOL, Japan) operated at 200 kV was used to examine the microstructure characteristics of the starting FWCNT powder, the Al-CNTs powder and the Al-CNTs composite. TEM samples of CNTs/Al composites were prepared using a focused ion beam (FIB) system (FB-2000S, HITACHI, Japan). Grain structure of each sample was also evaluated by electron backscatter diffraction (EBSD) using a TSL camera (TSL DigiView IV) attached to the FE-SEM. The texting sample surface is vertical to the axial direction of the extruded samples. The phase structures were identified by X-ray diffraction (XRD-6100, Shimazu, Japan). The instrument-induced XRD peak widening was investigated by the diffraction spectrum of a single-phase silicon plate (99.99% in purity). The full width at half maximum (FWHM) of the silicon (111) peak was measured to be 0.097°。

2.4. Tensile test

To evaluate the mechanical properties, room temperature tensile tests were carried out for each material along the extrusion direction. Tensile specimens were machined out from the extruded rods with a gauge length of 15 mm and a diameter of 3 mm. The tensile tests were performed on a universal testing machine (AUTOGRAPH AG-I 50 KN, Shimadzu Co. Ltd., Japan) at a strain rate of 5×10^{-4} s^{-1}. At least three specimens for each material were tested to assure reproducibility.

3. Results and discussion

The morphologies of the composite powders after HEBM for 24 h are shown in Fig. 2. It can be observed that the obtained powder particles have an average dimeter of ~20 μm (Fig. 2a),

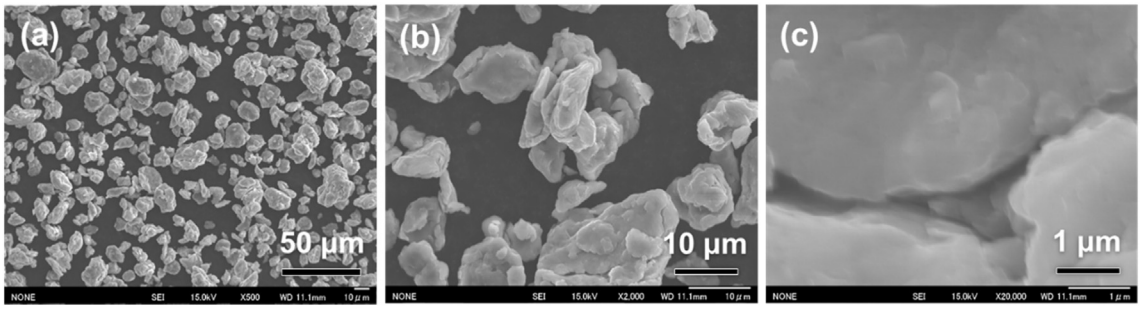

Fig. 2. Morphology of Al-1 wt.% FWCNTs composite powder after ball milling at different magnifications.

which is equivalent to that of starting powders. However, the composite powder particles exhibited a special shape, which is distinct from the tear-like shape of the starting powder [17]. From an enlarged view of the powder (Fig. 2b), it is seen that each composite powder particle consists of several parts. It suggested that the cold-welding phenomenon [19] occurred at the present HEBM condition. By previous experience, it can also be deduced that the Al-CNTs powder particles must experience the flattening, fracturing and cold-welding process during HEBM, which is similar to that of Al-MWCNTs powders at similar conditions [20].

To illustrate the effect of consolidation conditions on ball milled powders, the XRD patterns of the FWCNTs/Al composites (SPS500C and SPS600C) as well as the milled FWCNTs-Al powder are displayed in Fig. 3. Two significant characteristics could be found from the XRD patterns. First, a small amount of Al_4C_3 phase formed in the composites, as seen from the low intensity of Al_4C_3 peaks. The morphology of Al_4C_3 will be shown later. Second, the dislocation density (ρ) decreased from the as-milled powder to the SPS500C sample and then to the SPS600C sample, evidenced by the decrease of the FWHM of the Al (111) peak (Fig. 4). Since the grain size of the composites was measured as ~400 nm which was much larger than 100 nm, ρ can be estimated from Ref. [21].

$$\rho = \frac{\beta^2}{4.35b^2}\ , \tag{1}$$

where β is the true FWHM of Al(111) peak and b is the Burgers vector (0.29 nm) of Al. Moreover, $\beta = \beta_{measured} - \beta_{instrumental}$. The dislocation density of FWCNTs/Al (SPS500C) and FWCNTs/Al (SPS600C) can be estimated as $12.3 \times 10^{12}\ m^{-2}$ and $6.6 \times 10^{12}\ m^{-2}$. The noticeable decrease of dislocation density at higher temperature and longer time was attributed to the annealing effect during SPS on the stored dislocations in HEBM powders.

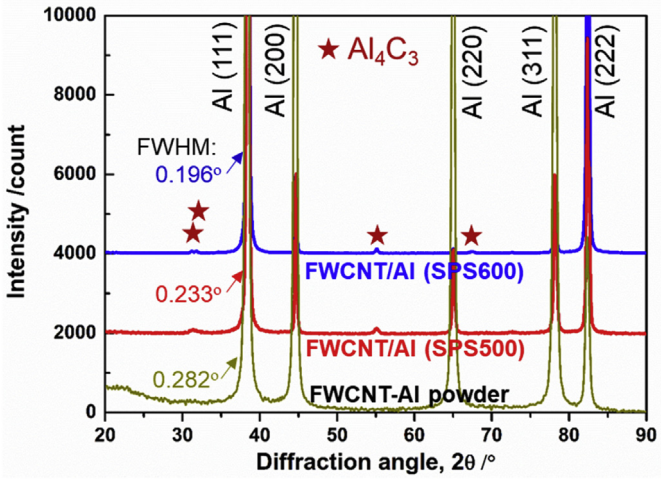

Fig. 3. XRD patterns of FWCNTs-Al powder and FWCNTs/Al composites with nominalized Al (111) peaks. FWHM is full width at half maximum of Al (111) peaks.

The grains and dislocation features are also investigated by EBSD (Fig. 4). It can be observed that in the FWCNTs/Al composites, the grain orientation is most pronounced at <111> (Fig. 4a and d), suggesting that the extruded materials exhibit a similar texture. This is in good agreement with the texture observations on extruded pure Al and MWCNTs/Al composites [22]. Comparing Fig. 4a and d, it is apparent that there is no significant difference in the grain orientation of SPS600C and SPS500C. However, as the SPS time and temperature increased, the final grain size increased for the extruded samples, where SPS600C had an average grain size of 0.46 μm and SPS500C had a value of 0.38 μm. The kernel average misorientation (KAM) figures that reflect the density of geometrically necessary dislocations are displayed for both FWCNTs/Al composites in Fig. 4c and f. It is clear that the SPS500C sample had a higher dislocation density level compared to SPS600C, shown as the overall decrease of the high dislocation density areas (in green color). This result confirmed the noticeable dislocation density difference measured from XRD peaks.

The dislocation morphology of the composites were further investigated by TEM. Fig. 5 shows the HRTEM images of FWCNTs/Al composite (SPS500C). Some dispersed FWCNTs were visible at the grain boundaries, as indicated by arrows in Fig. 5a. An enlarged view of a typical FWCNTs in black contrast is shown in Fig. 5b. The wall structure of FWCNTs (Fig. 1b) were hardly observed because of the overlap of Al and carbon atoms. There was no physical gap between Al and CNTs visible. From the atom planes of Al shown in Fig. 5c, a high dislocation density was observed at the matrix near FWCNTs.

Except for FWCNTs, Al_4C_3 was also detected in the SPS500C composite under TEM observation identified by selected area diffraction patterns (Fig. 6). The Al_4C_3 phases always exhibited as a nanorod shape and they sporadically distributed in Al matrix, which formed by a full consumption of FWCNTs. The TEM results on Al_4C_3 confirmed the small amount of Al_4C_3, in agreement with the XRD result (Fig. 3). The temperature of 500 °C was much lower than that required for Al_4C_3 formation, which is reported to be ~600 °C at the same route [23]. Yet, HEBM was applied in the present study while a mechanical coating process was used in Ref. [23]. HEBM could bring two effects to CNTs. One is an increased structural damage for CNTs in comparison to the mechanical coating process [24]. The other effect is that the HEBM process imposed severe plastic deformation on the Al powders, inducing a higher dislocation density in the Al matrix than the one by the coating process. These two effects promoted the interfacial reaction between Al and CNTs and resulted in the formation of Al_4C_3 nanorods at a relatively low temperature.

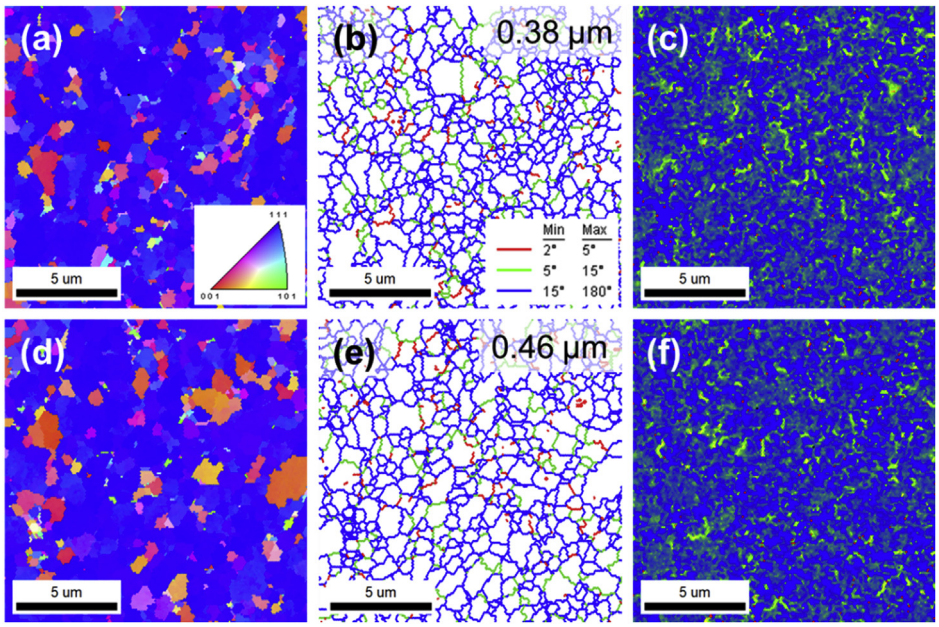

Fig. 4. EBSD analysis of FWCNTs/Al composite sintered at 500 °C for 30 min (a, b, c) and sintered at 600 °C for 60 min (d, e, f): inverse polar figures (a, d), grain misorientation angle maps (b, e) and kernel average misorientation (KAM) maps (c, f).

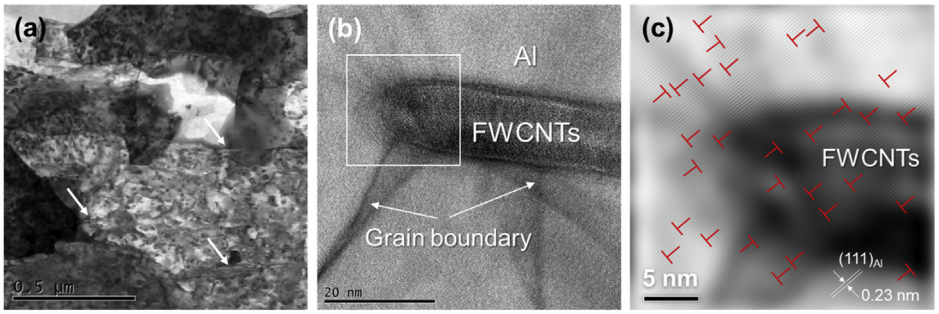

Fig. 5. HRTEM microstructures of FWCNTs/Al composite sintered at 500 °C for 30 min (SPS500C) at different magnifications. (c) is an inverse fast Flourier transformation image of the box area in (b).

In the SPS600 sample, individual Al_4C_3 nanorods with similar morphology were occasionally observed under TEM as well. However, it is difficult to compare the content of Al_4C_3 in these two composites by TEM because of the limited observation areas. As revealed in the previous study [25], the amount of Al_4C_3 precipitates increases in the composites processed by HEBM with increasing SPS temperature and time. It is thus understandable that, compared with SPS500C, more FWCNTs in SPS600C reacted with Al to form Al_4C_3. SPS conditions also have an obvious effect on the dislocation morphology in the composite. Fig. 7 shows the

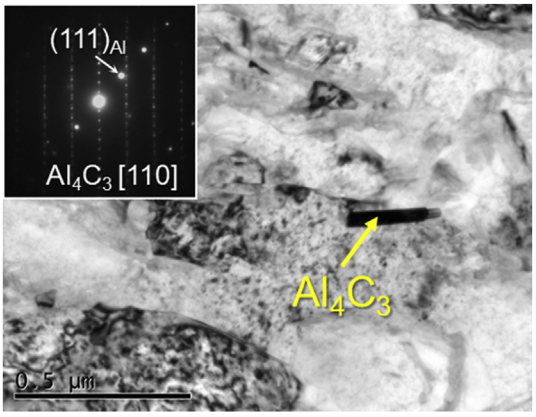

Fig. 6. TEM microstructures of FWCNTs/Al composite sintered at 500 °C for 30 min (SPS500C).

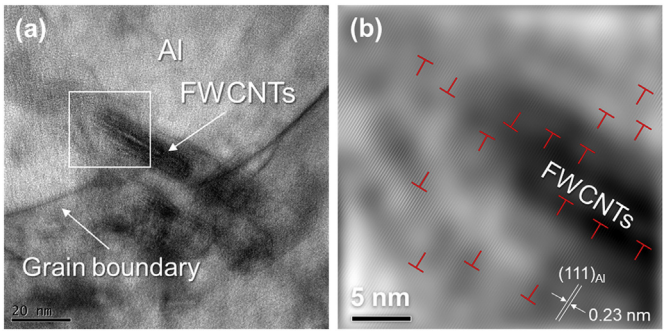

Fig. 7. TEM microstructures of FWCNTs/Al composite sintered at 600 °C for 60 min (SPS600C). (b) is an inverse fast Flourier transformation image of the box area in (a).

HRTEM images of the SPS600C composite sample. Compared with the 1%MWCNTs/Al composites processed by coating + SPS + hot extrusion [26], the dislocation density near the CNTs-matrix interface was much higher in the FWCNTs/Al (SPS600C) sample. In the present FWCNTs/Al (SPS600C) sample, the processing route is HEBM + SPS + hot extrusion and FWCNTs was used as the reinforcement. Therefore, the HEBM process and FWCNTs contribute to the increased dislocation density in FWCNTs/Al (SPS500C). Compared with the SPS500C sample (Fig. 5c), the dislocation density of SPS600C was much reduced, which was in good agreement with the measured dislocation values of these two composites by XRD.

Fig. 8a shows the nominal tensile stress-strain curves of FWCNTs/Al composites as well as referential Al materials sintered at different conditions. For both of the FWCNTs/Al SPS600C and SPS500C composites, over 100% and 60% strength increments were observed for yield strength (YS) and ultimate tensile strength (UTS), respectively, indicating a good strengthening effect of FWCNTs in AMCs. Especially, in the SPS500C composite, the improvement is 135% and 69% in YS and UTS, respectively. Compared with those sintered at 600 °C, both the samples sintered at 500 °C exhibited an increased strength. For example, SPS500C displayed an increase of 45 MPa in YS and of 40 MPa in UTS in comparison with SPS600C, which gave rise to a YS of 387 MPa and a UTS of 396 MPa. It should be noted that these two composites still possessed a good ductility with an elongation-to-failure over 10% (12% for SPS500C and 15% for SPS600C).

The tensile strength difference between the composites are mainly related to their grain size, dislocation density and the strengthening effect of FWCNTs. Taking YS into account, the strength difference ($\Delta\sigma$) of 45 MPa can be expressed as

$$\Delta\sigma = \Delta\sigma_{GS} + \Delta\sigma_{DD} + \Delta\sigma_{FWCNTs}, \quad (2)$$

where $\Delta\sigma_{GS}$, $\Delta\sigma_{DD}$ and $\Delta\sigma_{FWCNTs}$ are the increased strength contributed individually by grain size, dislocation density and FWCNTs. $\Delta\sigma_{GS}$ can be estimated according to the Hall-Petch formula [27]:

$$\Delta\sigma_{GS} = K\left(d_1^{-0.5} - d_2^{-0.5}\right), \quad (3)$$

where K is a constant (0.07 MPa $m^{0.5}$ for Al [28]), d_1 and d_2 are the average grain sizes of SPS500C and SPS600C, respectively. $\Delta\sigma_{GS}$ is thus calculated as 10.3 MPa. Considering dislocations strengthening, $\Delta\sigma_{DD}$ can be expressed as [29].

$$\Delta\sigma_{DD} = \alpha G b\left(\rho_1^{0.5} - \rho_2^{0.5}\right), \quad (4)$$

where α is a constant (1.25 for Al [29]), G is the shear modulus (25.4 GPa for Al [30]), b is the Burger's vector (0.286 nm for Al [30]), and ρ_1 and ρ_2 are the dislocation densities of SPS500C and SPS600C, respectively. $\Delta\sigma_{DD}$ is then calculated to be 11.2 MPa. Take $\Delta\sigma_{GS}$ and $\Delta\sigma_{DD}$ values into Eq. (2), $\Delta\sigma_{FWCNTs}$ is 23.5 MPa, which suggests that FWCNTs contributed extra 23.5 MPa more in the SPS500C than that in SPS600C, except for the differences caused by grain refinement and dislocation strengthening mechanisms. From recent studies [4,18,26], the strengthening mechanism of CNTs was attributed to load transfer and Orowan looping. Since SPS process did not change the size of FWCNTs, Orowan looping of FWCNTs did not make much difference in the two composites. Then higher strength in SPS500C implied larger load transfer effect in SPS500C. Based on the study of Kelly and Tyson [7], load transfer effect of fibrous FWCNTs is determined by the length to diameter ratio, interface bonding and volume fraction of FWCNTs. With decreasing SPS temperature and time, length to diameter ratio and the interface bonding conditions will not be improved [23]; however, the reaction between of FWCNTs and Al will be suppressed, leading to less FWCNTs transforming to Al_4C_3 and more remained FWCNTs. The results suggested that the integration of FWCNTs structure in the SPS500C composite was the key factor for the improved strength compared with the SPS600C composite.

Apart from the different tensile strengths, the two composites also had distinct strain hardening behavior, as seen from the tensile stress-strain curves in Fig. 8. To better understand the hardening behavior, the true stress-strain curves and normalized strain hardening rates for the two FWCNTs/Al materials were obtained, as shown in Fig. 9. It is seen that in the SPS500C necking occurs very early, and the true stress declined rapidly after necking, eventually to break. However, the necking stage lasted for ~0.1 of strain. While true yield strength of SPS600C is lower than that of SPS500C, the necking occurs much later. After the necking, the stress slowly decreases with an increase of strain.

To under the deformation behavior of SPS600C and SPS500C after yielding, the normalized strain hardening rate (Θ) versus strain is shown in the inset of Fig. 9. The normalized strain hardening rate (Θ) is defined as:

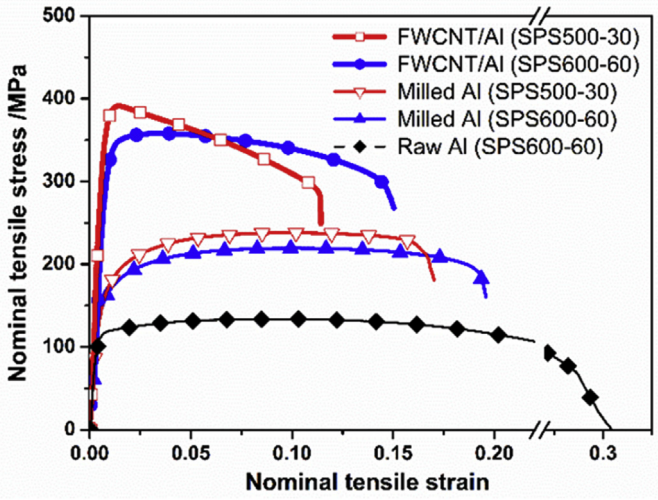

Fig. 8. Tensile properties of FWCNTs/Al composites and referential Al materials.

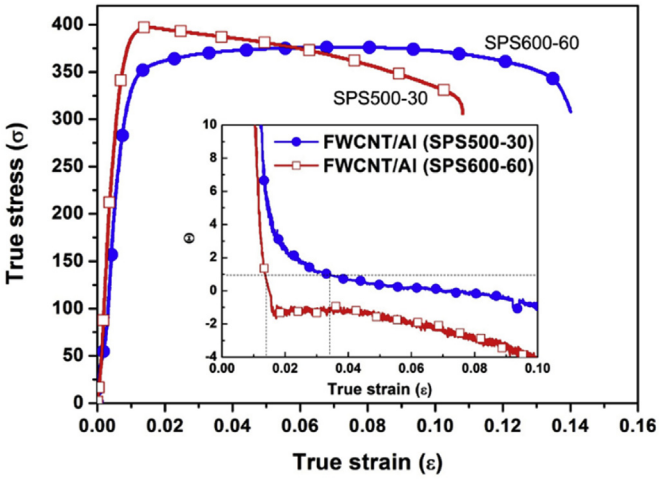

Fig. 9. Comparison between tensile true stress-strain curves of FWCNTs/Al composites sintered at two conditions. Inset shows strain hardening rate (Θ)-true strain curves.

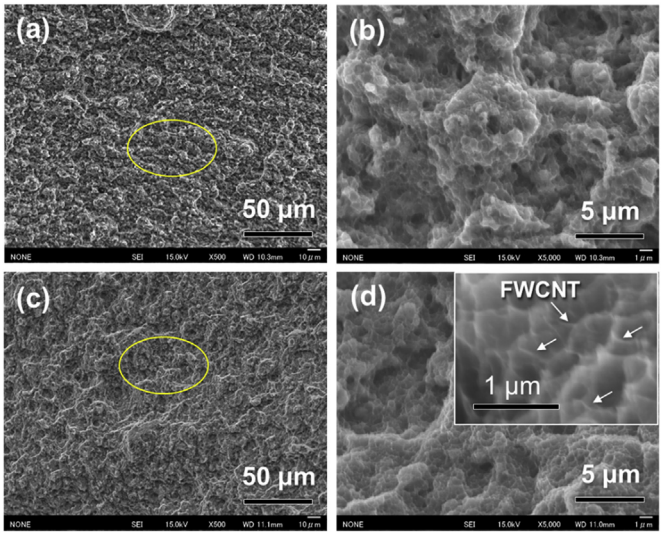

Fig. 10. Fracture morphologies of FWCNTs/Al composite sintered at 500 °C for 30 min (a, b) and sintered at 600 °C for 60 min (c, d). Inset of (d) shows a high-magnification view.

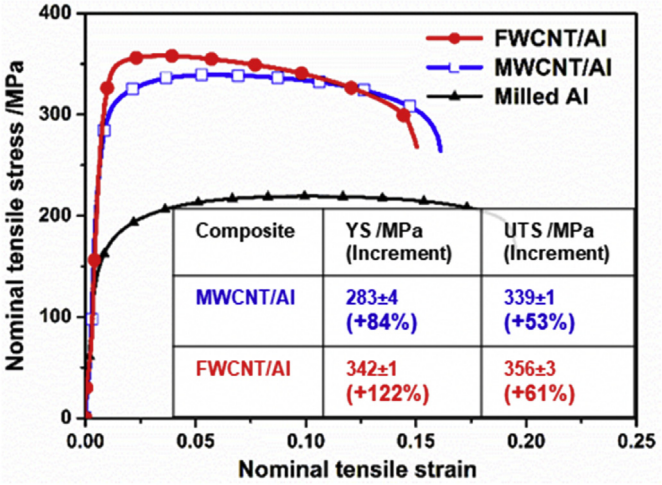

Fig. 11. Comparison between nominal tensile stress-strain curves of FWCNTs/Al and MWCNT/Al composites sintered at 600 °C for 60 min. Inset shows average tensile property values.

$$\Theta = \frac{1}{\sigma} \cdot \frac{d\sigma}{d\varepsilon}. \quad (5)$$

It can be observed that the normalized strain hardening rate of both materials after the yielding declined rapidly first and then slowly. According to Considère's criterion [11], when the strain hardening rate is equal to the true stress, $\frac{d\sigma}{d\varepsilon} = \sigma$, or $\Theta = 1$, necking will occur and the true stress begins to decrease until it breaks. Before the state of $\Theta = 1$, the material undergoes uniform deformation and thus the uniform elongation can be estimated at this point. The Θ of SPS500C composite (red curve in the inset of Fig. 9) falls fast and reaches the position of $\Theta = 1$ (horizontal dotted line in the figure) at uniform strain $\varepsilon_u = 0.014$ (inset of Fig. 9). This is consistent with the position of the necking in the true stress-true strain curve. After necking, SPS500C still has a comparatively large Θ stage of around −1, which causes the steady drop of true stress of the SPS500C. After the stable stage, Θ started to decrease

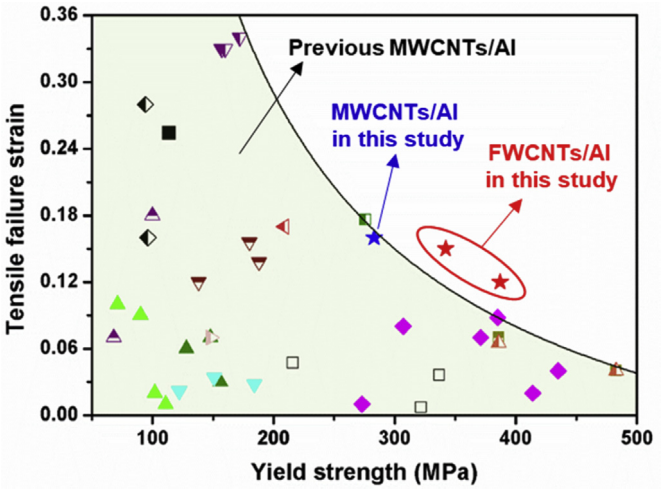

Fig. 12. Comparison between the tensile yield strength and failure strain of FWCNTs/Al and MWCNTs/Al composites in this study and previous MWCNTs/Al composites based on the data collected from recent review papers [4,31–33].

slowly and thus deformation could be sustained to a large deformation degree before failure (Fig. 9). With the SPS600C composite, necking occurred at around $\varepsilon = 0.034$, after which Θ decreased slowly and still maintained at comparatively large values, which enabled SPS600C to have a stable and long necking process (Fig. 9). The different strain softening behaviors in the two composites was probably due to the observed differences in grain size and dislocations. It can be concluded that, although the two composites had quite different strain hardening/softening behavior, the strain hardening/softening rates after necking in two composites still maintained at a high level. This fact resulted in good ductility of the two composites.

The fracture morphology of the FWCNTs/Al composites is shown in Fig. 10. On the fracture surfaces of the composites, fine and shallow dimples are clearly visible, which also confirms the excellent ductility. The dimple size was in sub-micrometer scale for both samples (Fig. 10b and d), which is basically coincident with the average grain size of the composites (Fig. 4). Moreover, dispersed FWCNTs were observed at the dimple boundaries (inset of Fig. 10d). Considering these facts, it is deduced that each dimple is corresponded to one matrix grain. Therefore, the fine grain size had a great effect on the deformation behavior and thus contributed to the good ductility of composites.

Fig. 11 shows the direct comparison between the tensile properties of AMCs reinforced with FWCNTs and MWCNTs sintered at 600 °C for 60 min. It is observed that FWCNTs/Al had higher YS and UTS than MWCNT/Al. Compared with the referential Al, the yield strength improvement in the MWCNTs/Al composites was remarkably improved from 84% to 122%. Suggesting the superior strengthening effect of FWCNT to MWCNTs. A comparison between the tensile properties of CNT/Al composites reported in this study and previous studies [4,31–33] is shown in Fig. 12. Compared with previous MWCNTs/Al composites, the two FWCNTs/Al composites in this work showed well-balanced strength and ductility. It suggests that FWCNTs are a good reinforcement candidate for MMCs with high mechanical performances.

4. Conclusions

In this study, FWCNTs were used as reinforcement in AMCs and its strengthening effect in composites was investigated. It was found that with decreasing SPS temperature and time, FWCNTs/Al

composites showed finer grains, increased dislocation density and improved structural integrity of FWCNTs, leading to increased tensile strength. The addition of 1 wt% FWCNTs led to 135% and 69% improvement in yield strength (YS) and ultimate tensile strength (UTS) of the referential Al material, respectively. It resulted in 387 MPa in YS, 396 MPa in UTS and 12% in elongation of a FWCNTs/Al composite. The good ductility was related to the ultra-fine grains and resulted comparatively high strain hardening rates after necking during tensile deformation. FWCNTs/Al composites developed in this study have improved balance of strength and ductility compared with conventional MWCNTs/Al composites.

Declaration of competing interest

The authors declare that they have no known competing financial interests or personal relationships that could have appeared to influence the work reported in this paper.

CRediT authorship contribution statement

B. Chen: Conceptualization, Investigation, Formal analysis, Writing - original draft, Supervision. **Z. Li:** Investigation, Writing - original draft. **J. Shen:** Investigation, Formal analysis. **S. Li:** Investigation, Formal analysis. **L. Jia:** Investigation, Formal analysis. **J. Umeda:** Resources. **K. Kondoh:** Formal analysis. **J.S. Li:** Supervision.

Acknowledgement

B. Chen would like to thank the financial supports from the National Natural Science Foundation of China (51901183), the Fundamental Research Funds for the Central Universities of Northwestern Polytechnical University (G2018KY0301), and the Research Fund of the State Key Laboratory of Solidification Processing (2019-TS-13).

References

[1] S.C. Tjong, Novel nanoparticle-reinforced metal matrix composites with enhanced mechanical properties, Adv. Eng. Mater. 9 (2007) 639–652.
[2] Y. Nishida, Introduction to Metal Matrix Composites, 2013.
[3] V.N. Popov, Carbon nanotubes: properties and application, Mater. Sci. Eng. R 43 (2004) 61–102.
[4] S.C. Tjong, Recent progress in the development and properties of novel metal matrix nanocomposites reinforced with carbon nanotubes and graphene nanosheets, Mater. Sci. Eng. R Rep. 74 (2013) 281–350.
[5] S.R. Bakshi, D. Lahiri, A. Agarwal, Carbon nanotube reinforced metal matrix composites - a review, Int. Mater. Rev. 55 (2010) 41–64.
[6] B. Chen, S. Li, H. Imai, L. Jia, J. Umeda, M. Takahashi, K. Kondoh, Load transfer strengthening in carbon nanotubes reinforced metal matrix composites via in-situ tensile tests, Compos. Sci. Technol. 113 (2015) 1–8.
[7] A. Kelly, W.R. Tyson, Tensile properties of fibre-reinforced metals: copper/tungsten and copper/molybdenum, J. Mech. Phys. Solid. 13 (1965), 329,in321,339-338,in322,350.
[8] R. Bacon, Growth, structure, and properties of graphite whiskers, J. Appl. Phys. 31 (1960) 283–290.
[9] A. Pantano, D.M. Parks, M.C. Boyce, Mechanics of deformation of single- and multi-wall carbon nanotubes, J. Mech. Phys. Solid. 52 (2004) 789–821.
[10] J. Stein, B. Lenczowski, E. Anglaret, N. Fréty, Influence of the concentration and nature of carbon nanotubes on the mechanical properties of AA5083 aluminium alloy matrix composites, Carbon 77 (2014) 44–52.
[11] A.M.K. Esawi, K. Morsi, A. Sayed, A.A. Gawad, P. Borah, Fabrication and properties of dispersed carbon nanotube–aluminum composites, Mater. Sci. Eng., A 508 (2009) 167–173.
[12] C. He, N. Zhao, C. Shi, X. Du, J. Li, H. Li, Q. Cui, An approach to obtaining homogeneously dispersed carbon nanotubes in Al powders for preparing reinforced Al-matrix composites, Adv. Mater. 19 (2007) 1128–1132.
[13] L. Jiang, G. Fan, Z. Li, X. Kai, D. Zhang, Z. Chen, S. Humphries, G. Heness, W.Y. Yeung, An approach to the uniform dispersion of a high volume fraction of carbon nanotubes in aluminum powder, Carbon 49 (2011) 1965–1971.
[14] F. Rikhtegar, S.G. Shabestari, H. Saghafian, Microstructural evaluation and mechanical properties of Al-CNT nanocomposites produced by different processing methods, J. Alloys Compd. 723 (2017) 633–641.
[15] A.M.K. Esawi, K. Morsi, A. Sayed, M. Taher, S. Lanka, The influence of carbon nanotube (CNT) morphology and diameter on the processing and properties of CNT-reinforced aluminium composites, Compos. Appl. Sci. Manuf. 42 (2011) 234–243.
[16] E.M. Byrne, M.A. McCarthy, Z. Xia, W.A. Curtin, Multiwall nanotubes can be stronger than single wall nanotubes and implications for nanocomposite design, Phys. Rev. Lett. 103 (2009), 045502.
[17] B. Chen, S. Li, H. Imai, L. Jia, J. Umeda, M. Takahashi, K. Kondoh, An approach for homogeneous carbon nanotube dispersion in Al matrix composites, Mater. Des. 72 (2015) 1–8.
[18] B. Chen, K. Kondoh, J.S. Li, M. Qian, Extraordinary reinforcing effect of carbon nanotubes in aluminium matrix composites assisted by in-situ alumina nanoparticles, Compos. B Eng. 183 (2020) 107691.
[19] A. Esawi, K. Morsi, Dispersion of carbon nanotubes (CNTs) in aluminum powder, Compos. Appl. Sci. Manuf. 38 (2007) 646–650.
[20] B. Chen, K. Kondoh, H. Imai, J. Umeda, Effect of initial state on dispersion evolution of carbon nanotubes in aluminium matrix composites during a high-energy ball milling process, Powder Metall. 59 (2016) 216–222.
[21] R. Chierchia, T. Böttcher, H. Heinke, S. Einfeldt, S. Figge, D. Hommel, Microstructure of heteroepitaxial GaN revealed by x-ray diffraction, J. Appl. Phys. 93 (2003) 8918–8925.
[22] B. Chen, S. Li, H. Imai, L. Jia, J. Umeda, M. Takahashi, K. Kondoh, Carbon nanotube induced microstructural characteristics in powder metallurgy Al matrix composites and their effects on mechanical and conductive properties, J. Alloys Compd. 651 (2015) 608–615.
[23] B. Chen, J. Shen, X. Ye, H. Imai, J. Umeda, M. Takahashi, K. Kondoh, Solid-state interfacial reaction and load transfer efficiency in carbon nanotubes (CNTs)-reinforced aluminum matrix composites, Carbon 114 (2017) 198–208.
[24] Z.Y. Liu, S.J. Xu, B.L. Xiao, P. Xue, W.G. Wang, Z.Y. Ma, Effect of ball-milling time on mechanical properties of carbon nanotubes reinforced aluminum matrix composites, Compos. Appl. Sci. Manuf. 43 (2012) 2161–2168.
[25] B. Chen, L. Jia, S. Li, H. Imai, M. Takahashi, K. Kondoh, In situ synthesized Al4C3Nanorods with excellent strengthening effect in aluminum matrix composites, Adv. Eng. Mater. 16 (2014) 972–975.
[26] B. Chen, J. Shen, X. Ye, L. Jia, S. Li, J. Umeda, M. Takahashi, K. Kondoh, Length effect of carbon nanotubes on the strengthening mechanisms in metal matrix composites, Acta Mater. 140 (2017) 317–325.
[27] N. Hansen, Hall–Petch relation and boundary strengthening, Scripta Mater. 51 (2004) 801–806.
[28] M.A. Meyers, K.K. Chawla, Mechanical Behavior of Materials, Cambridge university press, Cambridge, 2009.
[29] R. George, K.T. Kashyap, R. Rahul, S. Yamdagni, Strengthening in carbon nanotube/aluminium (CNT/Al) composites, Scripta Mater. 53 (2005) 1159–1163.
[30] H.J. Frost, M.F. Ashby, Deformation Mechanism Maps: the Plasticity and Creep of Metals and Ceramics, 1982.
[31] S.R. Bakshi, A. Agarwal, An analysis of the factors affecting strengthening in carbon nanotube reinforced aluminum composites, Carbon 49 (2011) 533–544.
[32] Z. Baig, O. Mamat, M. Mustapha, Recent progress on the dispersion and the strengthening effect of carbon nanotubes and graphene-reinforced metal nanocomposites: a review, Crit. Rev. Solid State Mater. Sci. (2016) 1–46.
[33] A.V. Radhamani, H.C. Lau, S. Ramakrishna, CNT-reinforced metal and steel nanocomposites: a comprehensive assessment of progress and future directions, Compos. Appl. Sci. Manuf. 114 (2018) 170–187.